IPN localizations of Konus short gamma-ray bursts

V. D. Pal'shin[1], K. Hurley[2], D. S. Svinkin[1], R. L. Aptekar[1], S. V. Golenetskii[1], D. D. Frederiks[1], E. P. Mazets[1], P. P. Oleynik[1], M. V. Ulanov[1], T. Cline[3,28], I. G. Mitrofanov[4], D. V. Golovin[4], A. S. Kozyrev[4], M. L. Litvak[4], A. B. Sanin[4], W. Boynton[5], C. Fellows[5], K. Harshman[5], J. Trombka[3], T. McClanahan[3], R. Starr[3], J. Goldsten[6], R. Gold[6], A. Rau[7], A. von Kienlin[7], V. Savchenko[8], D.M. Smith[9], W. Hajdas[10], S. D. Barthelmy[3], J. Cummings[11,29], N. Gehrels[3], H. Krimm[11,30], D. Palmer[12], K. Yamaoka[13], M. Ohno[14], Y. Fukazawa[14], Y. Hanabata[14], T. Takahashi[13], M. Tashiro[15], Y. Terada[15], T. Murakami[16], K. Makishima[17], M. S. Briggs[18], R. M. Kippen[12], C. Kouveliotou[19], C.Meegan[20], G. Fishman[19], V. Connaughton[18], M. Boër[21], C. Guidorzi[22], F. Frontera[22,31], E. Montanari[22,32], F. Rossi[22], M. Feroci[23], L. Amati[24], L. Nicastro[24], M. Orlandini[24] E. Del Monte[23], E. Costa[23], I. Donnarumma[23], Y. Evangelista[23], I. Lapshov[23], F. Lazzarotto[23], L. Pacciani[23], M. Rapisarda[23], P. Soffitta[23], G. Di Cocco[24], F. Fuschino[24], M. Galli[25], C. Labanti[24], M. Marisaldi[24], J.-L. Atteia[26], R. Vanderspek[27], G. Ricker[27]

[1]Ioffe Physical Technical Institute, St. Petersburg, 194021, Russian Federation

val@mail.ioffe.ru

[2]Space Sciences Laboratory, University of California, 7 Gauss Way, Berkeley, CA 94720-7450, USA

[3]NASA Goddard Space Flight Center, Greenbelt, MD 20771, USA

[4]Space Research Institute, 84/32, Profsoyuznaya, Moscow 117997, Russian Federation

[5]Department of Planetary Sciences, University of Arizona, Tucson, Arizona 85721, USA

[6]Applied Physics Laboratory, Johns Hopkins University, Laurel, MD 20723, USA

[7]Max-Planck-Institut für extraterrestrische Physik, Giessenbachstrasse, Postfach 1312, Garching, 85748 Germany

[8]ISDC Data Centre for Astrophysics, Chemin dEcogia 16, CH1290 Versoix, Switzerland

[9]Physics Department and Santa Cruz Institute for Particle Physics, University of California, Santa Cruz, Santa Cruz, CA 95064, USA

[10]Paul Scherrer Institute, 5232 Villigen PSI, Switzerland

[11]UMBC/CRESST/NASA Goddard Space Flight Center, Greenbelt, MD 20771, USA

[12]Los Alamos National Laboratory, Los Alamos, New Mexico 87545, USA

[13]Institute of Space and Astronautical Science (ISAS/JAXA), 3-1-1 Yoshinodai, Chuo-ku, Sagamihara, Kanagawa 252-5210, Japan

[14]Department of Physics, Hiroshima University, 1-3-1 Kagamiyama, Higashi-Hiroshima, Hiroshima 739-8526, Japan

[15]Department of Physics, Saitama University, 255 Shimo-Okubo, Sakura-ku, Saitama-shi, Saitama 338-8570, Japan

[16]Department of Physics, Kanazawa University, Kadoma-cho, Kanazawa, Ishikawa 920-1192, Japan

[17]Department of Physics, University of Tokyo, 7-3-1 Hongo, Bunkyo-ku, Tokyo 113-0033, Japan

[18]CSPAR and Physics Department, University of Alabama in Huntsville, Huntsville, AL 35899, USA

[19]Space Science Office, VP62, NASA Marshall Space Flight Center, Huntsville, AL 35812, USA

[20]Universities Space Research Association, 320 Sparkman drive, Huntsville, AL 35805

[21]Observatoire de Haute Provence (CNRS), 04870 Saint Michel l'Observatoire, France

[22]Physics Department, University of Ferrara, Via Saragat, 1, 44100 Ferrara, Italy

[23]INAF - Istituto di Astrofisica Spaziale e Fisica Cosmica, via Fosso del Cavaliere, Rome, I-00133, Italy

[24]INAF - Istituto di Astrofisica Spaziale e Fisica Cosmica di Bologna, via Gobetti 101, I-40129 Bologna, Italy

[25]ENEA-Bologna, Via Martiri Montesole, 4 I-40129 Bologna, Italy

[26]Université de Toulouse; UPS-OMP; CNRS; IRAP; 14, avenue Edouard Belin, F-31400 Toulouse, France

ABSTRACT

Between the launch of the *GGS Wind* spacecraft in 1994 November and the end of 2010, the Konus-*Wind* experiment detected 314 short-duration gamma-ray bursts (including 24 bursts which can be classified as short bursts with extended emission). During this period, the IPN consisted of up to eleven spacecraft, and using triangulation, the localizations of 276 bursts were obtained. We present the IPN localization data on these events.

Subject headings: catalogs - gamma-ray burst: general - techniques: miscellaneous

1. INTRODUCTION

Between 1994 November and 2010 December, the Konus gamma-ray spectrometer aboard the *GGS Wind* spacecraft detected 1989 cosmic gamma-ray bursts (GRBs) in the triggered mode, 314 of which were classified as short-duration gamma-ray bursts or short bursts with extended emission (EE). The classification was made basing on duration distribution of the unbiased sample of the 1168 Konus-*Wind* GRBs. Taking in account other characteristics of these short-duration bursts such as hardness ratio and spectral lag shows that about 16% of them can be in fact Type II (genuinely long) or at least their classification as Type I (genuinely short) is questionable. Nevertheless we consider here all 314 Konus-*Wind* short-duration and possible short-duration with EE bursts (hereafter we

[27]Kavli Institute for Astrophysics and Space Research, Massachusetts Institute of Technology, 70 Vassar Street, Cambridge, MA 02139, USA.

[29]Emeritus

[30]UMBC Physics Department 1000 Hilltop Circle Baltimore, MD 21250, USA

[31]Universities Space Research Association, 10211 Wincopin Circle, Suite 500, Columbia, MD 20144, USA

[32]INAF/Istituto di Astrofisica Spaziale e Fisica Cosmica di Bologna, via Gobetti 101, 40129 Bologna, Italy

[33]Istituto IS Calvi, Finale Emilia (MO), Italy

refer to them simply as Konus short bursts). Full details on the Konus-*Wind* GRB classification are given in Svinkin et al. (2013, in preparation).

Every Konus short burst detected was searched for in the data of the spacecraft comprising the interplanetary network (IPN). It has been found that 279 Konus-*Wind* short GRBs were observed by at least one other IPN spacecraft, enabling their localizations to be constrained by triangulation.

The IPN contained between 3 and 11 spacecraft during this period. They were, in addition to Konus-*Wind*: *Ulysses* (the solar X-ray/cosmic gamma-ray burst instrument, GRB), in heliocentric orbit at distances between 670 and 3180 lt-s from Earth (Hurley et al. 1992); the *Near-Earth Asteroid Rendezvous* mission (NEAR) (the remote sensing X-ray/Gamma-Ray Spectrometer, XGRS; Trombka et al. 1999), at distances up to 1300 lt-s from Earth; *Mars Odyssey* (the Gamma-Ray Spectrometer (GRS) that includes two detectors with GRB detection capabilities, the gamma sensor head (GSH), and the High Energy Neutron Detector (HEND); Boynton et al. 2004; Hurley et al. 2006), launched in 2001 April and in orbit around Mars starting in 2001 October, up to 1250 lt-s from Earth (Saunders et al. 2004); *Mercury Surface, Space Environment, Geochemistry, and Ranging* mission (MESSENGER) (the Gamma-Ray and Neutron Spectrometer, GRNS; Goldsten et al. 2007), en route to Mercury (in Mercury orbit since March 2011), launched in 2004 August, but commencing full operation only in 2007, up to ∼700 lt-s from Earth (Gold et al. 2001; Solomon et al. 2007); the *International Gamma-Ray Laboratory* (*INTEGRAL*) (the anti-coincidence shield ACS of the spectrometer SPI, SPI-ACS; Rau et al. 2005), in an eccentric Earth orbit at up to 0.5 lt-s from Earth; in low Earth orbits: the *Compton Gamma-Ray Observatory* (the Burst and Transient Source Experiment, BATSE; Fishman et al. 1992); *BeppoSAX* (the Gamma-Ray Burst Monitor, GRBM; Frontera et al. 1997); *the Ramaty High Energy Solar Spectroscopic Imager* (*RHESSI*; Lin et al. 2002; Smith et al. 2002); the *High Energy Transient Explorer* (*HETE-2*) (FREGATE; Ricker et al. 2003; Atteia et al. 2003); the *Swift* mission (the Burst Alert Telescope, BAT; Barthelmy et al. 2005; Gehrels et al. 2004); the *Suzaku* mission (the Wide-band All-sky Monitor, WAM; Yamaoka et al. 2009; Takashi et al. 2007); *AGILE* (MCAL and Super-AGILE) (Tavani et al. 2009); the *Fermi* mission (the Gamma-Ray Burst Monitor, GBM; Meegan et al. 2009), the *Coronas-F* solar observatory

(Helicon) (Oraevskii et al. 2002), the *Cosmos 2326* (Konus-A; Aptekar et al. 1998), *Cosmos 2367* (Konus-A2), and *Cosmos 2421* (Konus-A3) spacecraft, and the *Coronas-Photon* solar observatory (Konus-RF).

At least two other spacecraft recorded GRB detections during this period, although they were not used for triangulation and therefore were not, strictly speaking, part of the IPN. They are the *Defense Meteorological Satellite Program* (DMSP) (Terrell et al. 1996, 1998, 2004) and the *Stretched Rohini Satellite Series* (SROSS) (Marar et al. 1994).

We present the localization data obtained by the IPN for 276 of the 279 Konus-*Wind* short bursts observed by at least one other IPN s/c.

2. OBSERVATIONS

For each Konus short gamma-ray burst, a search was initiated in the data of the IPN spacecraft. For the near-Earth spacecraft and *INTEGRAL*, the search window was centered on the Konus-*Wind* trigger time, and its duration was somewhat greater than the *Wind* distance from Earth. For the spacecraft at interplanetary distances, the search window was twice the light-travel time to the spacecraft if the event arrival direction was unknown, which was the case for most events. If the arrival direction was known, even coarsely, the search window was defined by calculating the expected arrival time at the spacecraft, and searching in a window around it.

The mission timelines and the number of Konus-*Wind* short GRBs observed by each mission/instrument are shown in Figure 1. In this study, the largest number of bursts detected by an IPN instrument, after Konus, was 102, detected by *INTEGRAL* (SPI-ACS).

Table 1 lists the 279 Konus-*Wind* short GRBs observed by the IPN. The first column gives the burst designation, that is '`GRBYYYYMMDD_Tsssss`', where `YYYYMMDD` is the burst date, and `sssss` is the Konus-*Wind* trigger time (s UT) truncated to integer seconds. The next two columns give the burst date and Konus-*Wind* trigger time in the standard date and time formats. The 'Type' column specifies the burst type following the classification given in **?**. The types are: I (genuinely

short), II (genuinely long), I/II (the type is uncertain), Iee (short with extended emission), and Iee/II (the type is uncertain: short with extended emission or long with short precursor). The 'Time delay' column gives the propagation time delay from *Wind* to the Earth center and its 3σ uncertainty (they were calculated using the IPN localization, presented in this catalog: see section 6.3). The 'Observed by' column lists the IPN missions/instruments which observed the burst. The last two columns give the total number of the IPN s/c and the number of the distant IPN s/c which observed the burst.

During the period of consideration, four interplanetary s/c participated in the IPN: *Ulysses*, *NEAR*, *Mars Odyssey*, and *MESSENGER*. Table 2 gives the number of Konus short bursts observed by N distant s/c. The number of Konus short bursts observed by a total of N experiments, regardless of their distance from Earth, is given in Table 3 (the 35 bursts observed only by Konus-*Wind* have not been counted; detections by DMSP, and SROSS have been counted).

18 Konus short bursts were precisely localized by instruments with imaging capabilities, namely, *Swift*-BAT, *HETE-2* (WXM and SXC), and *INTEGRAL* IBIS/ISGRI. For most of these bursts an X-ray afterglow has been detected; for some of them a redshift z has been determined based on the optical afterglow or host galaxy spectroscopy. We have used these bursts to verify our IPN triangulations (see section 4.3).

3. METHODOLOGY

When a GRB arrives at two spacecraft with a delay δT, it may be localized to an annulus whose half-angle θ with respect to the vector joining the two spacecraft is given by

$$\cos\theta = \frac{c\delta T}{D} \tag{1}$$

where c is the speed of light and D is the distance between the two spacecraft. (This assumes that the burst is a plane wave, i.e. that its distance is much greater than D.)

The measured time delay has an uncertainty which is generally not symmetric $d_{\pm}(\delta T)$, i.e. the measured time delay can take values from $\delta T + d_{-}(\delta T)$ to $\delta T + d_{+}(\delta T)$ ($d_{-}(\delta T)$ is negative) at a

given confidence level.

The annulus half-widths $d\theta_{\pm}$, are

$$d\theta_{\pm} \equiv \theta_{\pm} - \theta = \cos^{-1}\left[\frac{c(\delta T + d_{\mp}(\delta T))}{D}\right] - \cos^{-1}\left[\frac{c\delta T}{D}\right] \tag{2}$$

It should be noted that even in case of symmetric error $|d_{-}(\delta T)| = d_{+}(\delta T)$, the annulus can still be significantly asymmetric if $c(\delta T + d_{\pm}(\delta T))/D \sim 1$ (i.e. the source is close to the vector joining the two spacecraft).

In case $d(\delta T) \ll D/c$ Eq. (2) reduces to commonly used expression:

$$d\theta_{\pm} = -\frac{cd_{\mp}(\delta T)}{D\sin\theta} \tag{3}$$

To derive the most probable time delay δT and its uncertainty $d_{\pm}(\delta T)$ we have used the χ^2 method described in Hurley et al. (1999a) for triangulations with distant s/c and this method with some modifications for Konus-*Wind*-near-Earth s/c (or *INTEGRAL*) triangulations.

Given a burst time history recorded by two instruments, the most probable time lag τ and its uncertainty $d_{\pm}(\tau)$ can be estimated as follows. Let $n_{1,i} = n(t_{1,i})$, $n_{2,j} = n(t_{2,j})$ and $\sigma_{1,i}$, $\sigma_{2,j}$ denote background-subtracted counts and their uncertainties measured by two instruments at evenly spaced intervals $t_{1,i} = t_{01} + i\Delta_1$, $t_{2,j} = t_{02} + j\Delta_2$, where $i = 0, .., m_1$, $j = 0, .., m_2$; and Δ_1, Δ_2 are the bin sizes and t_{01}, t_{02} are the absolute reference times (UT). To make things simpler, suppose $\Delta_1 = \Delta_2 = \Delta$. Usually one assumes Poisson statistics, so $\sigma_{1(2),i} = n^{1/2}_{tot1(2),i}$, where $n_{tot1(2),i}$ is total counts (source + background) in i-th bin. Let us assume that both time histories contain the burst of interest along with some intervals before and after it (if they do not exist they can always be added and padded by zeros with background variance), and $N+1$ bins from i_{start} contain the burst (or part of the burst we want to cross-correlate) in the second time history. Let construct the statistics:

$$R^2(\tau \equiv k\Delta) = \sum_{i=i_{start}}^{i=i_{start}+N} \frac{(n_{2,i} - sn_{1,i+k})^2}{(\sigma^2_{2,i} + s^2\sigma^2_{1,i+k})} \tag{4}$$

Where s is the scaling factor estimated as a ratio of the burst counts detected by the instruments $s = \sum_i n_{1,i} / \sum_j n_{2,j}$. In a perfect case of identical detectors, identical arrival angles, and Poisson

statistics, R^2 is distributed as χ^2 with N degrees of freedom (dof). In practice, there are several complicating factors. The detectors have different energy ranges, different response, and operate in different background environments. Fortunately, for short GRBs some of these complicated factors are less important: a) background variation on short time scales is small, and b) non-symmetric spectral evolution which produces a significant lag between light curves measured in different energy bands is almost absent in short GRBs (e.g. Norris, Scargle, & Bonnell 2001).

To account for all deflections from the perfect case we adopted the following approach: for a given number N (bins used to construct R^2) we calculate $\chi^2(N)$ corresponding to the 3σ confidence level (that is χ^2 for which the chi-square probability function $Q(\chi^2|N) = 2.7 \times 10^{-3}$), and adopt the corresponding 3σ level for reduced $R_r^2 (\equiv R^2/N)$ of

$$R^2_{r,3\sigma} = \chi^2_{r,3\sigma}(N) + R^2_{r,min} - 1 \tag{5}$$

where $R^2_{r,min}$ is the minimum of $R_r^2(\tau)$; 1 is subtracted, since $R^2_{r,min} \sim 1$ for the perfect case (in practice it is often > 1 and hence, $R^2_{r,3\sigma} > \chi^2_{r,3\sigma}(N)$). To identify the 3σ confidence interval for τ, we use the nearest points of the $R_r^2(\tau)$ curve above the 3σ level given by Eq. (5) - see the examples in Figure 2. After the time lag τ and its errors $d_\pm(\tau)$ have been found, the time delay and its uncertainty can be calculated as $\delta T = t_{02} - t_{01} + \tau$; $d_\pm(\delta T) = d_\pm(\tau)$ (here we assume there is no error in the absolute times t_{01} and t_{02}). For simplicity we will further refer to R^2 as χ^2.

4. LOCALIZATIONS: TRIANGULATION ANNULI

Using the above methodology one or more triangulation annuli have been obtained for 276 Konus-*Wind* short bursts. Specific details on time delay determination for different pairs of instruments are given in the subsections below.

4.1. Annuli involving distant s/c

Distant (interplanetary) spacecraft play an important role in GRB triangulation. Their long baselines make it possible to derive very small error boxes for many bursts. However, the detectors aboard these missions tend to be smaller than ones in orbits closer to Earth, and in some cases, are not dedicated GRB detectors, but rather, are planetary experiments which have GRB detection modes. Thus, they may have coarser time resolution and less sensitivity. Also, the spacecraft clocks on these missions are not always calibrated to UTC as accurately as the ones on missions closer to Earth (or their calibration cannot be determined as accurately). In the present catalog, the data of four interplanetary missions have been used: *Ulysses*, *NEAR*, *Mars Odyssey*, and *MESSENGER*. Of the four, only *Ulysses* had a dedicated GRB experiment. The time resolutions of the four ranged from 32 ms (*Ulysses*, triggered mode) to 1 s (*MESSENGER*, *NEAR*). When a short GRB is detected by an experiment with time resolution much greater than the burst duration, the result is usually an increase in the count rate in a single time bin, which means that the timing uncertainty is approximately one-half of the larger time resolution. The accuracy of the spacecraft clocks have been verified in two ways. For *Ulysses*, commands were sent to the GRB experiment at accurately known times, and, taking light-travel time and delays aboard the spacecraft into account, the timing could be verified to between several milliseconds and 125 milliseconds. (Although we believe that the timing was accurate to several milliseconds, technical issues often prevented us from verifying it.) In addition, the timing of all the interplanetary missions can be verified using triangulation of transient sources whose positions are well known by other means: SGRs are one possibility, and GRBs localized by *Swift*, for example, are another. For the purposes of this catalog, we have taken the extremely conservative approach that no 3σ cross-correlation uncertainty is less than 125 ms.

In total 146 Konus short bursts were observed by distant s/c: 30 by two distant s/c and 116 by one distant s/c. Among them 9 were precisely localized by instruments with imaging capabilities. We do not give here distant s/c annuli for these 9 bursts since they do not improve the precise localizations.

As a result 164 annuli have been obtained using the distant s/c data (two distant annuli for 27

bursts and one distant annulus for 110 bursts). Some of them have already been presented in the IPN catalogs: for BATSE bursts in Hurley et al. (1999a,b); **?**, for *BeppoSAX* bursts in Hurley et al. (2010), and for *HETE-2* bursts in Hurley et al. (2011b).

The histogram of Figure 3 shows the distribution of 3σ half-widths (HWs) of these 164 annuli. The smallest HW is $0\overset{\circ}{.}0024$ ($0.14'$), the largest is $2\overset{\circ}{.}21$, the mean is $0\overset{\circ}{.}093$ ($5.6'$), and the geometrical mean is $0\overset{\circ}{.}026$ ($1.6'$).

4.2. Annuli involving Konus-*Wind* and a near-Earth s/c

The Konus-*Wind* (hereafter *KW*) experiment plays a special role in the IPN thanks to the unique set of its characteristics: continuous coverage of the full sky by two omnidirectional spectrometers, orbit in interplanetary space that provides an exceptionally stable background, wide energy range (10 keV – 10 MeV nominal; ∼20 keV – 15 MeV at present time), and rather high sensitivity about 10^{-7} erg cm^{-2}. The duty cycle of the *KW*, defined as the time for data recovered divided by the total operational time of the experiment, is about 95%. It has observed most of the IPN events, providing an important vertex in the IPN at a distance of ≃1–7 lt-s (see Figure 5).

In the triggered mode *KW* records a burst time history in three energy ranges G1, G2, G3 with nominal bounds 10–50 keV, 50–200 keV, and 200–750 keV, with a variable time resolution from 2 ms up to 256 ms (for more details see Aptekar et al. (1995)). The time interval with the finest time resolution of 2 ms runs from T_0-0.512 s to T_0+0.512 s (T_0 is the trigger time) and in most cases covers the whole short burst, or at least its most intense pulse, thereby allowing very accurate cross-correlation with light curves of other instruments.

The *KW* clock is accurate to better than 1 ms, and this accuracy has been extensively verified by triangulation of many SGR bursts and GRBs.

The best results for cross-correlation with *KW* (i.e. minimum uncertainties in derived time delays) are provided by near-Earth s/c with high effective areas, namely *CGRO* BATSE, *BeppoSAX* GRBM, *INTEGRAL*-SPI-ACS, *Suzaku*-WAM, *Swift*-BAT, and *Fermi*-GBM.

At present, triangulation with *Fermi*-GBM usually provides the best result (the narrowest annulus) thanks to similar design of KW and GBM detectors (NaI scintillators), high effective area of GBM (several hundred cm^2 for combination of several NaI detectors), and photon time-tagging in 128 energy channels, that enables getting GBM light curves in the same energy ranges as KW light curves with any desired time binning.

Since the clocks of most of the near-Earth instruments are very accurate, high count statistics combined with fine time resolution often results in uncertainty in time delays as low as several milliseconds. Therefore, despite the rather small distance between KW and near-Earth s/c of several lt-s, the resulting relative error in time delay, $d_{\pm}(\delta T)/D$, which determines the width of the annulus (see Eq. (2,3)) can be comparable to or sometimes even smaller than for annuli involving distant s/c. Such small uncertainties of several ms, and hence narrow annuli, can be often derived for short bursts with sharp peaks or very steep rise and/or decay. On the other hand, bursts with smooth single-pulsed light curves usually give rather large cross-correlation uncertainties in time delays, and hence, rather wide triangulation annuli.

For *Wind*, *INTEGRAL*, and near-Earth s/c, ephemeris uncertainties are negligible compared to uncertainties in time delays and we do not take them in account.

In total 360 KW-near-Earth s/c annuli have been obtained. The histograms of Figure 4 shows the distributions of uncertainties in time delays and 3σ half-widths of these annuli. The smallest HW is $0\overset{\circ}{.}027$ ($1.6'$), the largest is $32\overset{\circ}{.}2$, the mean is $1\overset{\circ}{.}36$, and the geometrical mean is $0\overset{\circ}{.}45$.

Below some details on triangulation of the KW and the near-Earth s/c (and *INTEGRAL*) are given.

4.2.1. KW-CGRO (BATSE) triangulations

The Burst and Transient Source Experiment (BATSE) was a high energy astrophysics experiment aboard the *Compton Gamma Ray Observatory (CGRO)*. Its Large Area Detectors (LADs) measured a burst time history in four energy channels Ch1, Ch2, Ch3, Ch4, with approximate

channel boundaries: 25-55 keV, 55-110 keV, 110-320 keV, and >320 keV. The clock on the *CGRO* is accurate to 100 μs, and this accuracy was verified through pulsar timing. Onboard software increases the uncertainty in the BATSE trigger times to $\simeq$1 ms.

BATSE observed 55 *KW* short GRBs, 47 in the triggered mode, and 8 in the real-time mode. We derived *KW*-BATSE annuli for the all 47 *KW* short bursts observed in the triggered mode and for 6 bursts observed by BATSE in real-time mode (these bursts were observed by only *KW* and BATSE).

For cross-correlation with triggered BATSE bursts we utilized *KW* light curves in the G2+G3 or in the G2 band with 2 or 16-ms resolution and BATSE concatenated light curves (DISCLA, PREB, and DISCSC data types) in the Ch2+Ch3+Ch4 or in the Ch2+Ch3 band with a time resolution of 64 ms. For several GRBs such light curves are not available and we utilized other types of BATSE data. Usually we have tried different energy bands to check the consistency of the derived time delay and finally chose those with minimum χ^2. The cross-correlation curves for different bands may be slightly shifted relative each other (by several ms) but the 3σ intervals for cross-correlation lag τ are always in good agreement.

The resulting $\chi^2_{r,min}$ range from 0.06 to 4.51 with a mean of 0.81. The maximum $\chi^2_{r,min}$ of 4.51 (dof=6) is a clear outlier in the distribution of bursts over $\chi^2_{r,min}$. It corresponds to the exceptionally intense GRB19970704_T04097 (BATSE #6293) with a peak count rate of 180,000 counts s^{-1} (*KW* 2-ms time scale) and 688,000 counts s^{-1} (BATSE 64-ms time scale). Both light curves (*KW* and BATSE) must be significantly distorted due to dead-time and pile-up effects. The derived statistical uncertainty in the time delay is only 3 ms, so we added 6 ms systematic uncertainty to account for the distortions.

The derived uncertainties in the time delays range from 5 ms to 108 ms with a mean of 27 ms, and a geometrical mean of 20 ms. The resulting annuli 3σ half-widths range from $0\overset{\circ}{.}082$ to $11\overset{\circ}{.}0$ with a mean of $1\overset{\circ}{.}32$, and a geometrical mean of $0\overset{\circ}{.}66$. The widest annulus with half-width of $11\overset{\circ}{.}0$ was obtained for GRB19991001_T04950 (BATSE #7781) – at that time the *Wind* was at only 0.34 lt-s from Earth.

The distances between the center lines of the *KW*-BATSE annuli and the centers of BATSE locations range from 0.°007 to 7.°4 with a mean of 1.°96. For 14 bursts the BATSE error circle does not intersect the *KW*-BATSE annulus lying at the relative distance from the annulus (from the closest boundary of the annulus) ranging from 1.02σ to 15.8σ [1].

Of the 55 bursts, 16 were observed by only *KW* and BATSE, and 12 were observed by only *KW*, BATSE, and *BeppoSAX* (one of them was also observed by SROSS). For these bursts, we constrained the burst location to a segment of the *KW*-BATSE annulus using the following method. We assumed as the center of the segment the point on the annulus center line nearest to the center of the BATSE position, and then we derived the corners of the segment by intersection of the annulus and a circle centered at this point with a radius equal to the sum of twice the BATSE 1σ error and a systematic error, assumed to be a maximum of 2.°0 and the distance between the BATSE position and the center line of the annulus (a core systematic error of $\simeq 2^\circ$ was found for BATSE locations: see Briggs et al. (1999)). This is illustrated in Figure 6.

4.2.2. KW-Fermi (GBM) triangulations

The Gamma-Ray Burst Monitor (GBM) aboard the *Fermi* observatory is primarily designed to study of GRBs by making observations in the ∼8 keV – 40 MeV band (Meegan et al. 2009). The GBM has the advantage of high effective area and time-tagged data. The absolute timing of the GBM clock has an accuracy better than 20μs. The GBM TTE data contain counts in 128 energy channels from ∼5 keV to 2 MeV, that enables the preparation of the GBM light curve in three energy channels which are nearly the same as those of *KW*.

[1]For GRB19961225_T36436.638 (BATSE #5725) - the BATSE position given in the current BATSE catalog (R.A., Decl.(J2000), Err = 171.°31, -2.°85, 1.°5) is 25.°2 away from the center line of the 1.°6 wide *KW*-BATSE annulus. This GRB is a "mirror" case for BATSE, with a bimodal probability distribution for the location. The alternative solution is R.A., Decl.(J2000) = 141.°4, -5.°5, with a statistical error of 1.°8 (M. Briggs, private communication, 2011). This position is 7.°3 away from the center line of the *KW*-BATSE annulus. We use this alternative BATSE position in the paper.

GBM observed 34 *KW* short GRBs. We derived *KW*-GBM triangulation annuli for all of them.

For cross-correlation we utilized *KW* light curves in the G2+G3 or in the G2 band with 2 or 16-ms resolution and GBM light curves with 1 or 16 ms resolution made from the TTE data (only data of NaI detectors were used).

The resulting $\chi^2_{r,min}$ range from 0.16 to 2.10 with a mean of 0.90. The derived uncertainties in the time delays range from 2.5 ms to 136 ms with a mean of 22 ms, and a geometrical mean of 15 ms. The resulting annuli 3σ half-widths range from $0\overset{\circ}{.}035$ ($2.1'$) to $1\overset{\circ}{.}65$ with a mean of $0\overset{\circ}{.}35$, and a geometrical mean of $0\overset{\circ}{.}23$.

4.2.3. KW-INTEGRAL (SPI-ACS) triangulations

The Anti-Coincidence Shield (ACS) of the SPI instrument on-board *INTEGRAL*, besides serving to veto the background in the germanium spectrometer, is routinely used as a nearly omnidirectional detector for gamma-ray bursts (von Kienlin et al. 2003). It measures burst light curves with a time resolution of 50 ms in a single energy range above ∼80 keV (for more details see Lichti et al. (2000)). A systematic error in the ACS timing of 125±10 ms has been found (Rau et al. 2004) and all SPI-ACS lc have been corrected automatically for this error after 2004 April; corrections for it were applied by hand to the data prior to this date. Recently it was shown that the drift of ACS clock with respect to the germanium detector clock during the whole *INTEGRAL* mission is around 1 ms (Zhang et al. 2010), thereby reducing the systematic uncertainty in the ACS timing from 10 ms to 1 ms.

SPI-ACS observed 102 *KW* short GRBs. We derived *KW*-SPI-ACS annuli for 96 of them.

For cross-correlation we utilized *KW* light curves in the G2+G3 or in the G3 band with 2 or 16-ms resolution.

The resulting $\chi^2_{r,min}$ range from 0.04 to 3.96 with a mean of 1.02. The derived uncertainties

in the time delays range from 4 ms to 272 ms with a mean of 25 ms, and a geometrical mean of 19 ms. The resulting annuli 3σ half-widths range from $0\overset{\circ}{.}047$ ($2.8'$) to $6\overset{\circ}{.}9$ with a mean of $0\overset{\circ}{.}46$, and a geometrical mean of $0\overset{\circ}{.}30$.

4.2.4. KW-Suzaku (WAM) triangulations

The Wide-band All-sky Monitor (WAM) is the active shield of the Hard X-ray detector aboard the *Suzaku* mission (Yamaoka et al. 2009). In the triggered mode it measures light curves with a time resolution of 1/64 s in four energy channels which cover $\simeq$50–5000 keV range. In the real-time mode the time resolution is 1 s.

It was established that the *Suzaku*-WAM timing is consistent with negligible systematic uncertainties (Yamaoka et al. 2009).

WAM observed 67 *KW* short GRBs: 56 in the triggered mode and 11 in the real-time mode. We derived *KW*-WAM annuli for 49 triggered bursts.

For cross-correlation we utilized *KW* light curves in the G2+G3 or in the G3 band with 2 or 16-ms resolution and WAM light curves summed over four energy channels of 1 to 4 WAM detectors with the strongest response.

The resulting $\chi^2_{r,min}$ range from 0.21 to 1.78 with a mean of 1.00. The derived uncertainties in the time delays range from 4 ms to 120 ms with a mean of 23 ms, and a geometrical mean of 16 ms. The resulting annuli 3σ half-widths range from $0\overset{\circ}{.}060$ ($3.6'$) to $4\overset{\circ}{.}40$ with a mean of $0\overset{\circ}{.}44$, and a geometrical mean of $0\overset{\circ}{.}23$.

4.2.5. KW-BeppoSAX (GRBM) triangulations

The *BeppoSAX* Gamma-Ray Burst Monitor (GRBM) was the anticoincidence shield of the high energy experiment PDS (Phoswich Detection System; Frontera et al. 1997).

In the triggered mode it measured light curves with a time resolution of 7.8125 ms in the 40–700 keV range; in the real-time mode the time-resolution was 1 s (for more details see Frontera et al. 2009).

GRBM observed 53 *KW* short GRBs: 42 in the triggered mode and 11 in the real-time mode. We derived *KW*-GRBM annuli for 39 bursts observed in the triggered mode and for one burst observed in the real-time mode (this burst was observed by only *KW* and GRBM).

For cross-correlation we utilized *KW* light curves in the G2 or in the G2+G3 band with 2 or 16-ms resolution and GRBM light curves rebinned to 32 ms.

The resulting $\chi^2_{r,min}$ range from 0.25 to 12.1 with a mean of 1.44. The maximum $\chi^2_{r,min}$ of 12.1 (dof=6) is a clear outlier in the distribution of bursts over $\chi^2_{r,min}$. It corresponds to the exceptionally intense GRB19970704_T04097 with a peak count rate of 180,000 counts s^{-1} (*KW* 2-ms time scale) and 147,375 counts s^{-1} (GRBM 32-ms time scale). Both light curves (*KW* and GRBM) must be significantly distorted due to dead-time and pile-up effects. The derived statistical uncertainty in the time delay is only 2 ms, so we increased this uncertainty to 6 ms systematic uncertainty to account for the distortions.

The derived statistical uncertainties in the time delays range from 4.5 ms to 216 ms with a mean of 32 ms, and a geometrical mean of 18 ms.

Comparison of the initially derived annuli with other available IPN annuli as well as comparison of the GRBM and BATSE light curves for common bursts has revealed a systematic error in the GRBM timing up to 100 ms. Since this error varies from burst to burst (both in value and in sign), we had to introduce 100 ms systematic error for *KW*-SAX triangulations. That leads to significant broadening of the annuli, so their final 3σ half-widths range from $1\overset{\circ}{.}23$ to $32\overset{\circ}{.}2$ with a mean of $5\overset{\circ}{.}20$, and a geometrical mean of $3\overset{\circ}{.}71$.

4.2.6. KW-Swift (BAT) triangulations

The *Swift* Burst Alert Telescope (BAT) is a highly sensitive, large field of view (FOV) coded aperture telescope that detects and localizes GRBs in real time (Barthelmy et al. 2005). When a burst occurs outside its FoV, it can not be imaged, but the BAT light curve can be used for triangulation. For such bursts the 64 ms light curve in the four standard BAT energy channels (15–25 keV, 25–50 keV, 50–100 keV, and 100–350 keV) is always available. For some bursts, the TTE data are available, enabling any desired energy- and time- binning.

BAT observed 48 *KW* short bursts outside its FoV. We derived *KW*-BAT annuli for 24 of them.

For cross-correlation we utilized *KW* light curves in the G2 or in the G2+G3 band with 2 or 16-ms resolution and BAT 64 ms light curves usually taken in the energy range above 50 keV (which often provides the best S/N and better corresponds to the *KW* energy band).

The resulting $\chi^2_{r,min}$ range from 0.25 to 7.48 with a mean of 1.41. The maximum $\chi^2_{r,min}$ of 7.48 (dof=6) is a clear outlier in the distribution of bursts over $\chi^2_{r,min}$. It corresponds to the exceptionally intense GRB20060306_55358 with strong spectral evolution: a peak count rate of 187,000 counts s^{-1} (*KW* 2-ms time scale). The derived statistical uncertainty in the time delay is only 5 ms, so we added 10 ms systematic uncertainty.

The derived uncertainties in the time delays range from 5 ms to 124 ms with a mean of 27 ms, and a geometrical mean of 19 ms. The resulting annuli 3σ half-widths range from $0\overset{\circ}{.}059$ to $3\overset{\circ}{.}17$ with a mean of $0\overset{\circ}{.}53$, and a geometrical mean of $0\overset{\circ}{.}32$.

4.2.7. KW-Coronas-F (Helicon) triangulations

The Helicon gamma-ray spectrometer was one of the instruments onboard the *Coronas-F* solar space observatory (Oraevskii et al. 2002). It was similar to the *KW* spectrometer in the characteristics of its two detectors and in the data presentation structure. The similar design of

both instruments enabled good cross-correlation of measured burst light curves.

Helicon observed 14 *KW* short GRBs. We derived *KW*-Helicon annuli for all of them.

The resulting $\chi^2_{r,min}$ range from 0.25 to 2.67 with a mean of 1.02. The derived uncertainties in the time delays range from 4 ms to 80 ms with a mean of 25 ms, and a geometrical mean of 17 ms. The resulting annuli 3σ half-widths range from $0\overset{\circ}{.}045$ ($2.7'$) to $1\overset{\circ}{.}15$ with a mean of $0\overset{\circ}{.}38$, and a geometrical mean of $0\overset{\circ}{.}25$.

4.2.8. KW-Cosmos (Konus-A,A2,A3) triangulations

Konus-A, Konus-A2, and Konus-A3 were gamma-ray spectrometers aboard the *Cosmos* spacecraft 2326, 2367, and 2421, respectively. A brief description of the Konus-A instrument is given in Aptekar et al. (1998). Konus-A2, and Konus-A3 were similar to the Konus-A in the characteristics of its detectors and in the data presentation structure.

They observed 7 *KW* short GRBs in the triggered mode. We derived *KW*-*KA* annuli for 6 of them.

The resulting $\chi^2_{r,min}$ range from 0.73 to 1.42 with a mean of 1.00. The derived uncertainties in the time delays range from 4 ms to 56 ms with a mean of 34 ms, and a geometrical mean of 25 ms. The resulting annuli 3σ half-widths range from $0\overset{\circ}{.}15$ to $2\overset{\circ}{.}19$ with a mean of $1\overset{\circ}{.}02$, and a geometrical mean of $0\overset{\circ}{.}80$.

4.2.9. KW-RHESSI triangulations

The *Reuven Ramaty High-Energy Solar Spectroscopic Imager* (*RHESSI*) is a high resolution spectrometer designed to study high-energy emission from solar flares over a broad energy range from 3 keV to 17 MeV. The data are collected in the TTE mode enabling arbitrary energy and time binning.

RHESSI observed 61 *KW* short GRBs. We derived *KW*-HESSI annuli for 33 bursts.

For cross-correlation we utilized *KW* light curve in the G2, in the G1+G2, or in the G2+G3 band with 2, 16, 64, and 256-ms resolution (depending on burst intensity).

The resulting $\chi^2_{r,min}$ range from 0.36 to 2.62 with a mean of 1.06. The derived uncertainties in the time delays range from 2 ms to 184 ms with a mean of 38 ms, and a geometrical mean of 21 ms. The resulting annuli 3σ half-widths range from $0\overset{\circ}{.}027$ to $2\overset{\circ}{.}71$ with a mean of $0\overset{\circ}{.}57$, and a geometrical mean of $0\overset{\circ}{.}32$.

4.2.10. KW-HETE-2 (FREGATE) triangulations

The gamma-ray detector of *HETE-2*, called FREGATE, was designed to detect gamma-ray bursts in the energy range 8-400 keV.

In the triggered mode it measures light curves with a time resolution of 1/32 s in the 8–400 keV range; in the real-time mode the time-resolution is 0.1638 s.

FREGATE observed 10 *KW* short bursts in the triggered mode and 9 *KW* short GRBs in the real-time mode. In most cases the FREGATE response is significantly weaker than responses of other instruments flying on low-Earth s/c, so we used the FREGATE data only for a few cases when no other low-Earth s/c detected the burst. We derived *KW-HETE* annuli for 5 bursts observed in the triggered mode and for 1 burst observed in the real-time mode (it was observed by only *KW* and FREGATE).

For cross-correlation we utilized *KW* light curve in the G2 or in the G2+G3 band with 2 or 16-ms resolution.

The resulting $\chi^2_{r,min}$ range from 0.50 to 1.62 with a mean of 1.09. The derived uncertainties in the time delays range from 36 ms to 168 ms with a mean of 93 ms. The resulting annuli 3σ half-widths range from $0\overset{\circ}{.}50$ to $2\overset{\circ}{.}37$ with a mean of $1\overset{\circ}{.}22$.

4.2.11. KW-AGILE (MCAL) triangulations

The mini-calorimeter (MCAL) aboard the *AGILE* mission is a spectrometer sensitive to gamma-rays in the energy band $\simeq$0.35 – 100 MeV. MCAL has the advantage of time-tagged data.

MCAL observed 20 *KW* short GRBs in the triggered mode and 1 *KW* short GRB in the real-time mode. In many cases the MCAL response is rather weak due to its high energy threshold and strong attenuation by the GRID instrument, so we used the MCAL data only for several intense bursts. In total we derived 8 *KW*-MCAL annuli.

For cross-correlation we utilized *KW* light curve in the G3 or in the G2+G3 band with 2 or 16-ms resolution.

The resulting $\chi^2_{r,min}$ range from 0.29 to 1.44 with a mean of 0.80. The derived uncertainties in the time delays range from 5 ms to 21 ms with a mean of 13 ms. The resulting annuli 3σ half-widths range from $0\overset{\circ}{.}071$ ($4.3'$) to $0\overset{\circ}{.}244$ with a mean of $0\overset{\circ}{.}168$.

4.3. Verifying triangulation annuli

Of the 276 Konus short bursts localized by IPN, 18 were precisely localized by instruments with imaging capabilities: 15 by *Swift*-BAT (one of them, GRB 091005, was also localized by *Fermi*-LAT), 2 by *HETE-2* (WXM and SXC), and 1 by *INTEGRAL* IBIS/ISGRI.

We utilized these bursts to verify our triangulations. For these 18 bursts, 23 *KW*-near-Earth s/c and 12 *KW-INTEGRAL* annuli were obtained (we have not used the light curves of the instruments which imaged the burst, since the instrument response for imaged bursts is different from those detected outside the FoV and used for IPN triangulations). In each case the triangulation annuli are in agreement with the known position of the source, thereby confirming the reliability of our triangulations. Indeed, such tests constitute "end-to-end" calibrations, as they confirm not only spacecraft timing and ephemeris information, but also, the cross-correlations of the various time histories and derivations of the annuli.

The histograms of Figure 7 shows the distribution of relative source offsets from the center lines of the annuli. One can see that all offsets (in absolute values) are less than 2σ. The minimum offset of the precise position is -2.0σ, the maximum is 1.9σ, the average is 0.04σ, and the standard deviation is 1.1σ.

5. LOCALIZATIONS: ADDITIONAL CONSTRAINS

In addition to triangulation annuli, several other types of localization information are included in this catalog. They are ecliptic latitude range, autonomous burst localizations obtained by *CGRO* BATSE, *BeppoSAX* GRBM, and *Fermi* GBM, and Earth- or Mars- blocking (MESSENGER is in an eccentric orbit around Mercury, so Mercury-blocking is quite rare). This additional information helps constrain the triangulation position i.e. to choose one of two triangulation boxes, or to eliminate portions of a single annulus.

5.1. Ecliptic latitudes

The ecliptic latitudes of the bursts are derived by comparing the count rates of the two *KW* detectors taken in the waiting mode with 1.472 s or 2.944 s time resolution. The axis of the detector S2 points towards the north ecliptic pole, and the axis of the S1 points toward the south ecliptic pole. In addition to statistical uncertainties, the ecliptic latitude determination is subject to systematic uncertainties due to, among other things, time-variable cosmic X-ray sources and absorption by other instruments aboard the spin-stabilized *Wind* spacecraft. The estimated ecliptic latitudes can be taken to be at the 95% confidence level.

The ecliptic latitude range, namely the best estimate of b, and the lower and upper limits b_{min}, b_{max} can be considered as an annulus centered at the north or south ecliptic pole, with a half-angle $\theta = 90^\circ - |b|$ and its half-widths $d_-(\theta) = b_{min} - b$, $d_+(\theta) = b_{max} - b$.

5.2. Planet-blocking

Planet-blocking is specified by the right ascension and declination of the planet's center and its radius. When a spacecraft in low Earth or Mars orbit observes a burst, the planet blocks up to ≈ 3.7 sr of the sky. The source position must be outside this occulted part of the sky.

The allowed part of the sky can be described as a degenerate annulus centered at the direction opposite to the planet's center, with a half-angle $\theta = 0$ whose widths $d_-(\theta) = 0$, $d_+(\theta) = \sin^{-1}(R_{planet}/R)$, where R is the radius of the s/c orbit (here we neglect the oblateness of the planet).

5.3. Autonomous localizations

A principle of autonomous burst localization using a system of detectors posessing anisotropic angular sensitivity was suggested by Golenetskii et al. (1974) and first implemented in the KONUS instruments on Venera 11 and 12 missions (Mazets & Golenetskii 1981).

Similar localization systems consisting of different numbers of detectors have been placed on *CGRO* (BATSE), *BeppoSAX* (GRBM), and *Fermi* (GBM). These autonomous localizations, derived by comparing the count rates of various detectors, are affected by Earth albedo and absorption by spacecraft materials, among other things, and their shapes are in general complex. The error circles are approximations to these shapes. They are centered at the point which is the most likely arrival direction for the burst, and their radii are defined so that their areas are equal to the 1σ(BATSE, GBM) or 90% confidence (GRBM) statistical-only true error regions. All these localizations also have systematic errors of several degrees or more.

These error circles can also be described as degenerate annuli centered at the most likely arrival direction for the burst, with a half-angle $\theta = 0$ whose widths $d_-(\theta) = 0$, $d_+(\theta) = r$, where r is the positional error.

6. LOCALIZATIONS: RESULTS

Table 4 summarizes localization information for 276 Konus short bursts. The first column gives the burst designation (see Table 1). The second column gives the number of localization constraints (the number of rows with localization information for the burst). The six subsequent columns give localizations expressed as a set of annuli: the third column gives the source of the location: either sc1–sc2 (triangulation annulus derived using sc1 and sc2), or 'EclBand' (range of ecliptic latitudes), or 'Instr' (name of the instrument which autonomously localized the bursts), or 'Planet' (planet-blocking); columns 4–8 list the right ascension and declination of the annulus center (J2000), the annulus radius θ, and the 3σ uncertainties in the radius $d_-(\theta)$, $d_+(\theta)$.

Planet-blocking is given only if it constrains the location. The ecliptic latitude range is given for all bursts. All available autonomous localizations are given.

The *Swift*-BAT localizations are taken from the second *Swift* BAT catalog covering 2004 December 19 to 2009 December 21 (Sakamoto et al. 2011), and for the latest bursts from the GCN Circulars with BAT refined positions.

The *HETE-2* localizations for GRB 040924 (=GRB20040924_T42735) and GRB 060121 (=GRB20060121_T80700) are taken from Fenimore et al. (2004) and Arimoto et al. (2006), respectively.

The IBIS/ISGRI localization for GRB 070707 (=GRB20070707_T58122) is taken from Götz et al. (2007).

The BATSE localizations are taken from the current catalog on the BATSE website [2], as well as from the BATSE untriggered burst catalogs (Stern et al. 2001; Kommers et al. 2000)[3].

---

[2]http://www.batse.msfc.nasa.gov/batse/grb/catalog/current/

[3]Since the catalog by Stern et al. (2001) contains the localizations for all 8 Konus short bursts detected by BATSE in the real-time mode, and the catalog by Kommers et al. (2000) misses some of them, the given localizations are solely from Stern et al. (2001).

The *BeppoSAX* localizations are taken either from the GRBM catalog (Frontera et al. 2009) or from the IAU and GCN Circulars.

The GBM localizations are taken from the first *Fermi* GBM catalog covering 2008 July 12 to 2010 July 11 (Paciesas et al. 2012), the GCN Circulars, or from the latest version of corresponding 'glg_tcat*.fit' file in the GBM data archive [4].

6.1. Boxes

For those bursts which were detected by three or more well separated s/c, a triangulation box can be derived.

In general, the intersection of two annuli involving distant s/c gives a small box with an area as small as 1 arcmin^2.

The intersection of two annuli derived from a distant s/c, Konus-*Wind*, and a near-Earth s/c usually gives an elongated box, which nevertheless in most cases has a small area of several hundred arcmin^2. In some cases the intersection of annuli derived from a single distant s/c, Konus-*Wind*, and a near-Earth s/c can give a smaller error box than annuli derived using two distant s/c.

Long boxes were derived for bursts not observed by any distant s/c, but observed by *KW*, *INTEGRAL* SPI-ACS, and one or more near-Earth s/c. In such cases, the box is formed by a *KW*–near-Earth s/c annulus and an *INTEGRAL*–near-Earth s/c annulus, or by a *KW*–near-Earth s/c annulus and a *KW*–*INTEGRAL* annulus intersecting at grazing incidence.

In all cases, if the three s/c which formed the box were nearly aligned, the annuli intersect at grazing incidence, resulting in a long box.

In total we derived 162 error boxes for Konus short bursts: 27 for bursts observed by two distant s/c, 84 for bursts observed by one distant s/c and at least one near-Earth s/c, and 51 for

[4]ftp://legacy.gsfc.nasa.gov/fermi/data/gbm/bursts

bursts observed by only *KW*, *INTEGRAL*, and one or more near-Earth s/c. In some cases these error regions are actually long arcs rather than boxes (in particular this is a case when burst was not observed by a distant s/c), but for simplicity we still refer to them as boxes since they are formed by intersection of two or more triangulation annuli.

6.2. Segments

For those bursts which were detected by only *KW* and another s/c, or by *KW* and one or more near-Earth s/c, the resulting localization is formed by a triangulation annulus (the narrowest in the case of several *KW*-near-Earth s/c annuli) and additional constraints. These localizations represent whole annulus (in the case where it is entirely inside the allowed ecliptic latitude band and there are no other constraints) or one or two annulus segments, formed by intersection of the annulus with the ecliptic latitude band, and/or by exclusion of the occulted part of the annulus, or by combination with the BATSE localization (see section 4.2.1).

In 96 bursts had this kind of localization: 26 were bursts observed by *KW* and a distant s/c (of these, 3 were also observed by a near-Earth s/c in real-time mode, but *KW*-near-Earth s/c annuli have not been derived for them), and 70 were bursts observed by only *KW* and one or more near-Earth s/c.

6.3. Resulting error regions

Table 5 gives the description of the final IPN error regions for 258 Konus short bursts (this sample does not include the 18 imaged bursts). The eight columns contain the following information: (1) the burst designation (see Table 1), (2) the number of error regions for the burst: 1 or 2, (3) the region type: 'B' (box), 'lB' (long box: box with maximum dimension $> 10^\circ$), 'S' (segment), or 'A' (annulus), (4) the right ascension of the center of the error region, in the first row, and the right ascensions of the four corners in the following four rows, and (5) the declination of the center of the error region, in the first row, and the declinations of the four corners in the following four

rows, (6) the area (for two regions the sum of their areas), (7) the maximum dimension (that is the maximum angular distance between two points at the region boundary; for segments larger than half an annulus, this is just the outer diameter of the annulus), (8) the list of the annuli and additional constraints from Table 4 which were used to form the region(s). All coordinates are J2000.

In general, a simple, four-corner error region description is inaccurate and the curvature of the annuli should be taken into account. Only in cases where the maximum dimension of the error region is less than several degrees, can the box be reasonably well represented by its four corners. In other cases, especially when the region is a long arc or annulus segment, the given corners and center are intended to roughly indicate the position of the region on the sky. Figures showing the IPN localization (all derived annuli and the resulting error region(s)) can be found at the Ioffe Web site [5].

A histogram of IPN error region areas is shown in Figure 8. For bursts observed by distant s/c the areas range from 2.40×10^{-4} sq. deg (0.86 arcmin^2) to 71.7 sq. deg with a mean of 1.87 sq. deg, and a geometrical mean of 0.135 sq. deg. For bursts without distant s/c detections the areas range from 0.207 sq. deg to 2785 sq. deg with a mean of 154 sq. deg, and a geometrical mean of 28.4 sq. deg.

7. COMMENTS ON SPECIFIC EVENTS

GRB 051103 (=GRB20051103_T33943) may in fact be a giant SGR flare in the nearby M81 group of interacting galaxies as was suggested by Frederiks et al. (2007). The final IPN localization of this event along with further exploration of this possibility are given in Hurley et al. (2010).

GRB 070201 (=GRB20070201_T55390) is likely a giant SGR flare from the Andromeda galaxy (Mazets et al. 2008).

[5] http://www.ioffe.ru/LEA/tmp/ShortGRBs_IPN/Figures_All.pdf

GRB 000420 (=GRB20000420_T422714): based on the *KW-NEAR* annulus it was suggested by Ofek (2007) that this burst might be associated with the nearby Sc-type galaxy M74 (NGC 628). The position of this galaxy lies well outside the wide *KW-SAX* annulus thereby excluding it as a possible host for this short GRB – see Figure 9.

GRB 990405 (=GRB19990405_T30059): initially this event was classified as a burst from SGR 1900+14 since the narrow *SAX-Ulysses* annulus (3σ half-width of $0\overset{\circ}{.}035$) passes through the position of this SGR. The derived wide *KW-SAX* annulus (3σ half-width of $6\overset{\circ}{.}4$) is also consistent with the SGR position. But this burst is substantially harder even than two unusually hard bursts from SGR 1900+14: 981022, 991001 (Woods et al. 1999), making the possible association of this burst with the SGR doubtful.

8. SUMMARY AND CONCLUSION

We have presented the most comprehensive IPN localization data on 276 Konus-*Wind* short bursts. For 258 bursts IPN error regions were obtained and for 18 bursts precisely localized by instruments with imaging capability IPN triangulation annuli were derived for calibration purposes.

In total we derived 524 triangulation annuli, including 164 annuli with distant s/c.

It was shown that for many shorts bursts *KW*–near-Earth s/c (or *INTEGRAL*) triangulation yields a rather narrow annulus (with half-width sometimes comparable to or even better than the annuli using distant s/c data), thereby providing small error boxes with areas of several hundred arcmin^2 even for those *KW* short bursts which were detected by only one distant s/c (and one or more near-Earth s/c), and providing a long box in cases where the burst was detected by Konus-*Wind*, *INTEGRAL* SPI-ACS, and one or more near-Earth s/c.

The localizations can be used for a wide variety of purposes, including searches for a) gravitational wave and neutrino signals from merging compact objects b) very high energy photons from the burst sources c) giant SGR flares in nearby galaxies.

This paper continues a series of catalogs of gamma-ray burst localizations obtained by arrival time analysis, or "triangulation" between the spacecraft in the 3rd interplanetary network, as summarized in Table 6.

The Konus-*Wind* experiment is supported by a Russian Space Agency contract and RFBR grant 12-02-00032a. K.H. is grateful for IPN support under the following NASA, JPL, and MIT grants and contracts. JPL 958056 and 1268385 (Ulysses); NNX07AH52G (ADA); NAG5-12614, NNG04GM50G, NNG06GE69G, NNX07AQ22G, NNX08AC90G, NNX08AX95G and NNX09AR28G (INTEGRAL); NNG05GTF72G, NNG06GI89G, NNX07AJ65G, NNX08AN23G, NNX09AO97G, and NNX10AI23G (Swift); NAG5-3500 and NAG5-9503 (NEAR); MIT-SC-R-293291 and NAG5-11451 (HETE-II); JPL 1282043 (Odyssey); NNX06AI36G, NNX08AB84G, NNX08AZ85G, NNX09AV61G, NNX10AR12G (Suzaku); NNX09AU03G (Fermi); NNX07AR71G (MESSENGER); NAG5-7766, NAG5-9126, and NAG5-10710 (BeppoSAX).

REFERENCES

Arimoto, M., et al. 2006, GCN Circ. 4550

Aptekar, R., et al. 1995, Space Sci. Rev. 71, 265

Aptekar, R., et al. 1998, ApJ 493, 404

Atteia, J.-L., et al., 2003, in Gamma-Ray Burst and Afterglow Astronomy 2001, A Workshop Celebrating the First Year of the HETE Mission, Eds. G. Ricker and R. Vanderspek, AIP Conf. Proc. 662 (AIP: New York), 17

Barthelmy, S. D., et al. 2005, Space Sci. Rev. 120, 143

Boynton, W. V., et al. 2004, Space Sci. Rev. 110, 37

Briggs, M. S., et al. 1999, ApJS 122, 503

Celidonio, G., et al. 1998, IAUC 6851

Fenimore, E. E., et al. 2004, GCN Circ. 2735

Feroci, M., et al., 1997, in EUV, X-Ray, and Gamma-Ray Instrumentation for Astronomy VIII, Eds. O. Siegmund and M. Gummin, SPIE 3114, 186

Frederiks, D. D., et al. 2007, Astronomy Lettrs, 33, 19

Fishman, G., Meegan, C., Wilson, R., Paciesas, W., and Pendleton, G., 1992, in Proc. Compton Observatory Science Workshop, Eds. C. Shrader, N. Gehrels, and B. Dennis, NASA Conf. Publication 3137, 26

Frontera, F., et al. 1997, Astron. Astrophys. Suppl. Ser. 122, 357

Frontera, F., et al. 2009, ApJS 180, 192

Gehrels, N., et al. 2004, ApJ611, 1005

Gold, R., et al. 2001, Planetary and Space Sci. 49, 1467

Golenetskii, S. V., Il'Inskii, V. N., & Mazets, E. P. 1974, Cosmic Research, 12, 706

Goldsten, J. O., et al. 2007, Space Sci. Rev. 131, 339

Götz, D., et al. 2007, GCN Circ. 6608

Groot, P., et al. 1998, IAUC 6852

Hurley, K., et al. 1992, Astron. Astrophys. Suppl. Ser. 92(2), 401

Hurley, K., et al. 1998, GCN Circ.53

Hurley, K., et al. 1999a, ApJS 120, 399

Hurley, K., et al. 1999b, ApJS 122, 497

Hurley, K., et al. 2000a, ApJ 533, 884

Hurley, K., et al. 2000b, ApJ 534, 258

Hurley, K., et al. 2000c, ApJS 128, 549

Hurley, K., et al. 2005, ApJS 156, 217

Hurley, K., et al. 2006, ApJS 164, 124

Hurley, K., et al. 2010, MNRAS 403, 342

Hurley, K., et al. 2011, ApJS 196, 1

Hurley, K., et al. 2011, ApJS 197, 34

Hurley, K., et al. 2013, arXiv:1110.6470

Jager, R., et al. 1997, Astron. Astrophys. Suppl. Ser. 125, 557

von Kienlin, A., et al. 2003, A&A, 411, L299

Kommers, J., Lewin, W., Kouveliotou, C., van Paradijs, J., Pendleton, G., Meegan, C., and Fishman, G., 2000, ApJ533, 696

Laros, J., et al. 1997, ApJS 110, 157

Laros, J., et al. 1998, ApJS 118, 391

Lichti, G. G., et al. 2000, in The Fifth Compton Symposium, Eds. Mark L. McConnell & James M. Ryan, AIP Conf. Proc. 510 (AIP: New York), p. 722

Lin, R. P., et al. 2002, Sol. Phys., 210, 3

Marar, T., et al., 1994, A&A 283, 698

Mazets, E. P., and Golenetskii, S. V., 1981, Astrophys. Space Sci. 75, 47

Mazets, E. P., et al., 2008, ApJ 680, 545

Meegan, C., et al., 2009, ApJ 702, 791

Norris, J. P., Scargle, J. D., and Bonnell, J. T. 2001, in Gamma-Ray Bursts in the Afterglow Era, ed. E. Costa, F. Frontera, & J. Hjorth (Berlin: Springer), 40

Ofek, E. O. 2007, ApJ 659, 339

Oraevskii, V. N., Sobelman, I. I., Zhitnik, I. A., and Kuznetsov, V. D., 2002, Phys. Usp. 45, 886

Pacieas, W. S., et al. 2012, ApJS, 199, 18

Rau, A., et al. 2004, GCN Circ. 2568

Rau, A., von Kienlin, A., Hurley, K., and Lichti, G. 2005, A&A 438, 1175

Ricker, G., et al., 2003, in Gamma-Ray Burst and Afterglow Astronomy 2001, A Workshop Celebrating the First Year of the HETE Mission, Eds. G. Ricker and R. Vanderspek, AIP Conf. Proc. 662 (AIP: New York), 3, 2003

Sakamoto, T., et al., 2011, ApJS 195, 2

Saunders, R. S., et al., 2004, Space Sci. Rev. 110, 37

Smith, D., et al., 1999, ApJ 526, 683

Smith, D. M. et al. 2002, Sol. Phys. 210, 33

Solomon, S. C., et al., 2007, Space Sci. Rev. 131, 3

Stern, B., Tikhomirova, Y., Kompaneets, D., Svensson, R., and Poutanen, J., 2001, ApJ563, 80

Tavani, M., et al., 2009, A&A 502, 995

Takashi, T., et al., 2007, PASJ 59, S35

Terrell, J., Lee, P., Klebesadel, R., and Griffee, 1996, in 3rd Huntsville Symposium, AIP Conf. Proc. 384 (AIP: New York), Eds. C. Kouveliotou, M. Briggs, and G. Fishman, 545

Terrell, J., Lee, P., Klebesadel, R., and Griffee, J., 1998, in Gamma-Ray Bursts, 4th Huntsville Symposium, Eds. C. Meegan, R. Preece, and T. Koshut, AIP Conf. Proc. 428, AIP Press (New York), p. 54

Terrell, J., and Klebesadel, R., 2004 , in Gamma-Ray Bursts: 30 Years of Discovery, Eds. E. Fenimore and M. Galassi, AIP Conf. Proc. 727 (AIP: New York), p. 541

Trombka, J., et al., 1999, Nucl. Inst. And Methods in Physics Research A 422, 572

Yamaoka, K., et al., 2009, PASJ 61, S35

Vetere, L., Soffitta, P., Massaro, E., Giommi, P., and Costa, E., 2007, A&A 473, 347

Woods, P. M., et al., 1999, ApJ, ApJ, 527, L47

Zhang, X.-L., Rau, A., & von Kienlin, A. 2010, 8th INTEGRAL Workshop The Restless Gamma-ray Universe September 27-30, Dublin, Ireland

Table 1. IPN/Konus short gamma-ray bursts

Designation	Date	Konus-*Wind* trigger time (UT)	Type[a]	Time delay[b] (s)	Observed by[c]	N_{tot}[d]	N_{dist}[e]
GRB19950210_T08424	1995 Feb 10	02:20:24.148	I	-2.602(-0.009,+0.007)	Uly(T),GRO(#3410)	3	1
GRB19950211_T08697	1995 Feb 11	02:24:57.749	I	0.003(-0.009,+0.005)	Uly(T),GRO(#3412),SRS(T)	4	1
GRB19950414_T40882	1995 Apr 14	11:21:22.798	I	0.350(-0.008,+0.006)	Uly(R)	2	1
GRB19950419_T08628	1995 Apr 19	02:23:48.860	I	0.418(-0.030,+0.026)	Uly(T)	2	1
GRB19950523_T31302	1995 May 23	08:41:42.284	I	0.436(-0.068,+0.040)	Uly(T)	2	1

[a]Burst type as given in Svinkin et al. (2013, in preparation)

[b]Propagation time delay from *Wind* to the Earth center and its 3σ uncertainty. This delay should be added to the Konus-*Wind* trigger time to get the Earth-crossing time.

Note. — Table 1 will be published in its entirety in the electronic edition of the Astrophysical Journal Supplement Series. A portion is shown here for guidance regarding its form and content.

[c]AGI: *Astro-rivelatore Gamma a Immagini LEggero* (AGILE); GRO: *Compton Gamma-Ray Observatory*; DMS: *Defense Meteorological Satellite Program*; Fer: *Fermi*; Hel: Helicon-*Coronas-F*; HET: *HETE-2*; INT: *International Gamma-Ray Laboratory* (INTEGRAL); KA1: Konus-A on *Cosmos 2326*; KA2: Konus-A2 on *Cosmos 2367*; KA3: Konus-A3 on *Cosmos 2421*; KRF: Konus-RF on *Coronas-Photon*; MES: *Mercury Surface, Space Environment, Geochemistry, and Ranging* mission; MO: *Mars Odyssey*; NEA: *Near Earth Asteroid Rendezvous* mission; RHE: *Ramaty High Energy Solar Spectroscopic Imager*; SAX: *BeppoSAX*; SRS: *Stretched Rohini Satellite Series*; Suz: *Suzaku*; Swi: *Swift*; Uly: *Ulysses*; XTE: *Rossi X-Ray Timing Explorer*;
In parentheses the detection mode is given: T – trigger, R – rate increase; #n – trigger number (when available)

[d]Total number of IPN spacecraft which observed the burst (including Konus-*Wind*)

[e]Number of distant IPN spacecraft (i.e., *NEAR*, *Mars Odyssey*, *MESSENGER*, *Ulysses*) which observed the burst

Table 2. Number of Konus short bursts observed by N distant spacecraft, i.e., *NEAR*, *Mars Odyssey*, *MESSENGER*, and *Ulysses*

N=0	1	2
133	116	30

Table 3. Number of Konus short bursts in this catalog observed by a total of N experiments, regardless of their distance from Earth

N=1	2	3	4	5	6	7	8	9
0	77	80	63	37	13	6	2	1

Table 4. IPN localization data

Designation	N	Location [a] source	R.A.(J2000) (deg)	Decl.(J2000) (deg)	θ (deg)	$d_-(\theta)$ (deg)	$d_+(\theta)$ (deg)
GRB19950210_T08424	4	Uly-BATSE	155.444	25.745	53.632	-0.008	+0.008
		Kon-BATSE	130.358	18.848	52.331	-0.153	+0.119
		EclBand	90.000	-66.561	43.3	-19.5	+46.0
		BATSE	154.55	-27.48	0	0	1.15
GRB19950211_T08697	4	Uly-BATSE	335.804	-25.124	85.830	-0.006	+0.006
		Kon-BATSE	311.587	-18.236	89.959	-0.068	+0.122
		EclBand	270.000	66.561	65.5	-39.5	+22.6
		BATSE	9.51	52.65	0	0	1.08

[a] sc_1-sc_2 – IPN annulus obtained using sc_1 and sc_2 data; EclBand – the ecliptic latitude band of the burst; sc – spacecraft/instrument which autonomously localized the burst (the abbreviations are given in Table 1)

Note. — Table 4 will be published in its entirety in the electronic edition of the Astrophysical Journal Supplement Series. A portion is shown here for guidance regarding its form and content.

Table 5. IPN error regions

Designation	n	Type[a]	R.A.(J2000)[b] (deg)	Decl.(J2000)[b] (deg)	Max. dim. (deg)	Area (sq. deg)	Formed by[c]
GRB19950210_T08424	1	B	154.645	-27.879	0.606	9.44E-3	Uly-GRO,KW-GRO,EclBand
			154.287	-27.880			
			154.972	-27.890			
			155.002	-27.875			
			154.318	-27.865			
GRB19950211_T08697	1	B	14.943	+53.759	0.346	4.36E-3	Uly-GRO,KW-GRO,EclBand
			15.168	+53.673			
			14.688	+53.871			
			14.717	+53.844			
			15.196	+53.645			

[a]Type of the error region: 'B' (box), 'lB' (long box: maximum dimension > 10°), 'S' (annulus segment), and 'A' (whole annulus).

[b]For localizations which are an entire annulus, these fields are empty (and only one row for the burst is given). The parameters of the annuli can be found in Table 4.

[c]The localization data from Table 4 used to form the box.

Note. — Table 5 will be published in its entirety in the electronic edition of the Astrophysical Journal Supplement Series. A portion is shown here for guidance regarding its form and content.

Table 6. Recent IPN catalogs of gamma-ray bursts

Years covered	Number of GRBs	Description
1990–1992	16	*Ulysses, Pioneer Venus Orbiter,* WATCH, SIGMA, PHEBUS GRBs[a]
1990–1994	56	*Granat*-WATCH supplement[b]
1991–1992	37	*Pioneer Venus Orbiter, Compton Gamma-Ray Observatory, Ulysses* GRBs[c]
1991–1994	218	BATSE 3B supplement[d]
1991–2000	211	BATSE untriggered burst supplement[e]
1992–1993	9	*Mars Observer* GRBs[f]
1994–1996	147	BATSE 4Br supplement[g]
1994–2010	279	Konus short bursts[h]
1996–2000	343	BATSE 5B supplement[i]
1996–2002	475	*BeppoSAX* supplement[j]
2000–2006	226	HETE-2 supplement[k]
2008–2010	146	GBM supplement[l]

[a]Hurley et al. (2000a)

[b]Hurley et al. (2000c)

[c]Laros et al. (1998)

[d]Hurley et al. (1999a)

[e]Hurley et al. (2005)

[f]Laros et al. (1997)

[g]Hurley et al. (1999b)

[h]present catalog

[i]Hurley et al. (2011a)

[j]Hurley et al. (2010)

[k]Hurley et al. (2011b)

[l]Hurley et al. (2013)

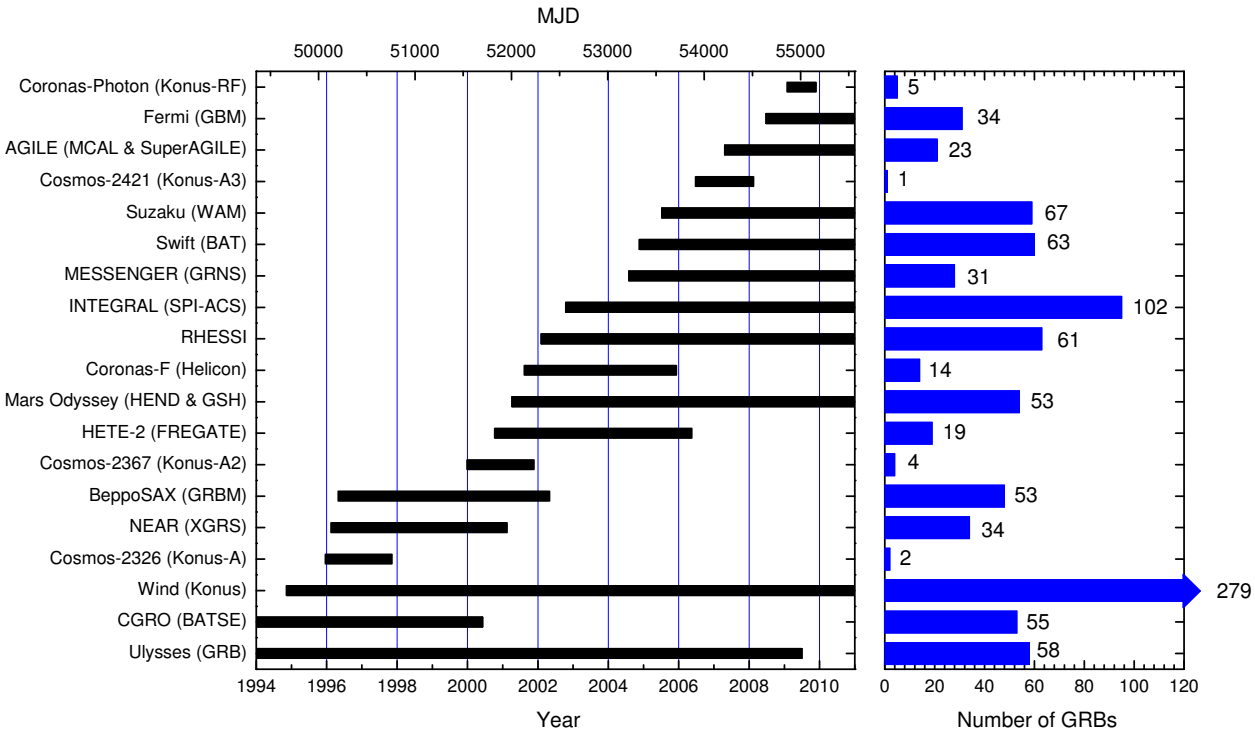

Fig. 1.— *Left*: Timelines of the IPN missions since the launch of *Wind* in 1994, November (instrument names are given in the parentheses). *Right:* Number of Konus short bursts observed by each mission (for *Wind* (Konus) – the number of bursts observed by at least one other IPN s/c is given).

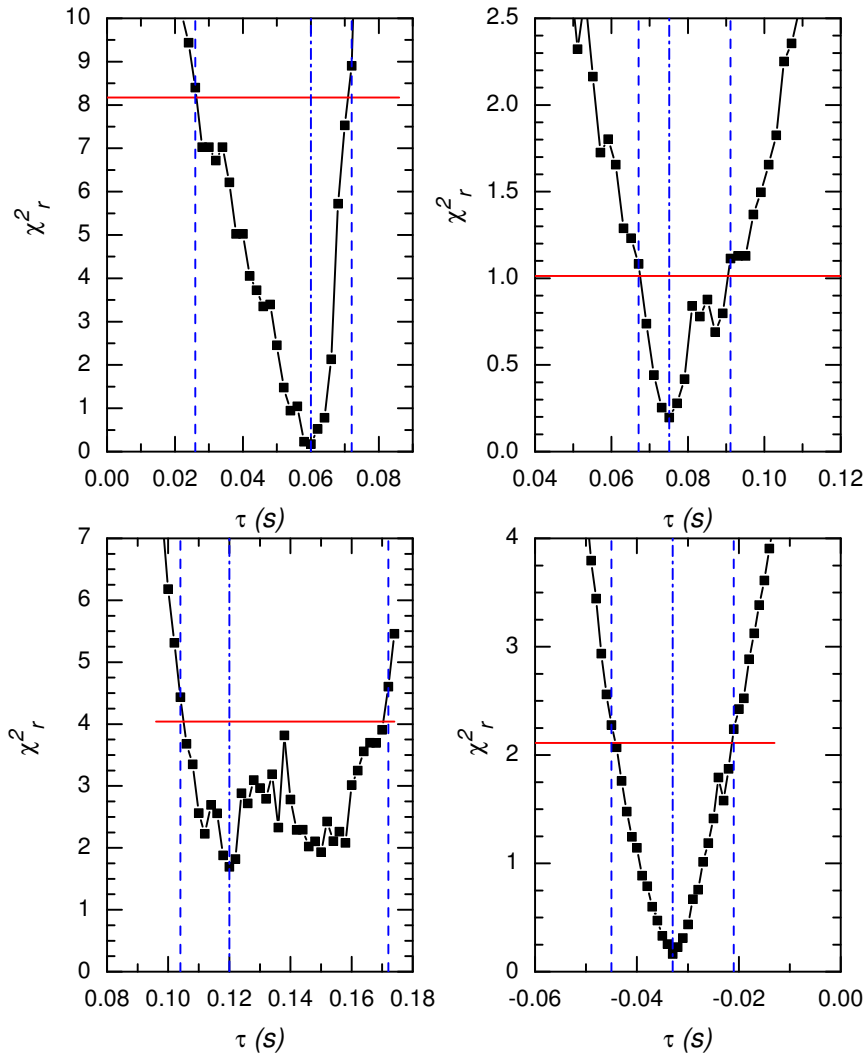

Fig. 2.— Examples of cross-correlation curves $\chi^2_r(\tau)$. Horizontal red lines denote 3σ levels. Vertical blue lines show the best cross-correlation time lag τ (dashed-dotted line) and its 3σ confidence interval (dashed lines). *Top Left:* GRB19971118_T29008. Cross-correlation of the *KW* 2 ms light curve with the BATSE 64 ms light curve; $\tau = 0.060(-0.034, +0.012)$ s (dof=2). *Top Right:* GRB20070321_T67937. Cross-correlation of the *KW* 2 ms light curve with the WAM 1/64 s light curve; $\tau = 0.075(-0.008, +0.016)$ s (dof=12). *Bottom Left:* GRB20090715_T62736. Cross-correlation of the *KW* 2 ms light curve with the SPI-ACS 50 ms light curve; $\tau = 0.120(-0.016, +0.052)$ s (dof=7). *Bottom Right:* GRB20100206_T48606. Cross-correlation of the GBM 1 ms light curve with the *KW* 16 ms light curve; $\tau = -0.033 \pm 0.012$ s (dof=9).

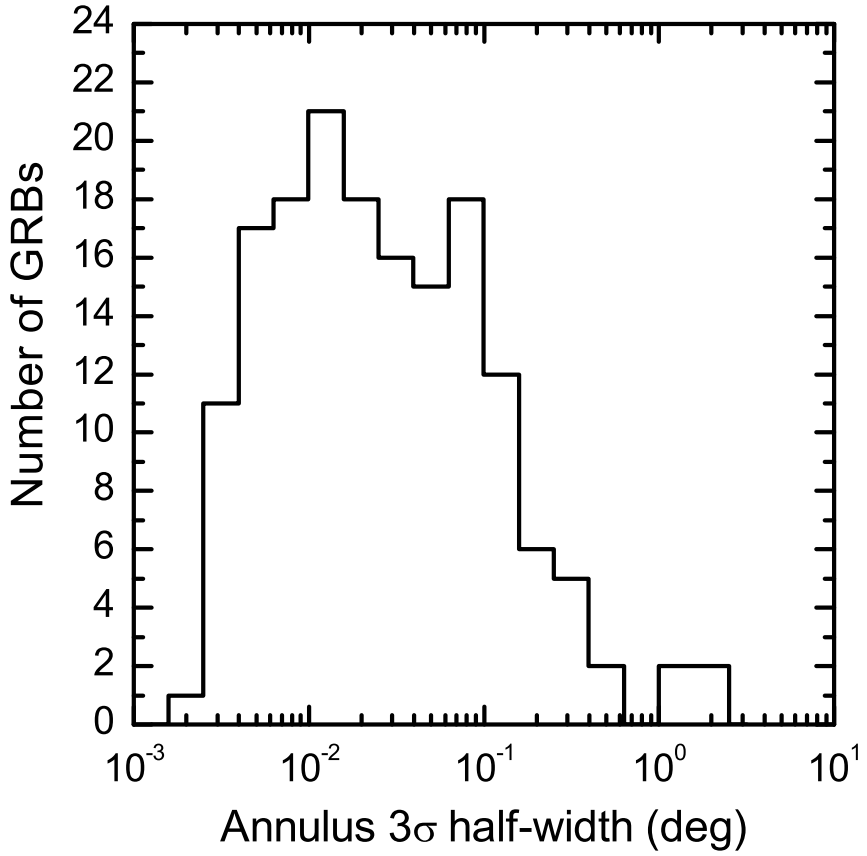

Fig. 3.— Distribution of 3σ half-widths (HWs) of the 164 triangulation annuli obtained using the distant s/c data. The smallest HW is $0\overset{\circ}{.}0024$ ($0.14'$), the largest is $2\overset{\circ}{.}21$, the mean is $0\overset{\circ}{.}093$ ($5.6'$), and the geometrical mean is $0\overset{\circ}{.}026$ ($1.6'$).

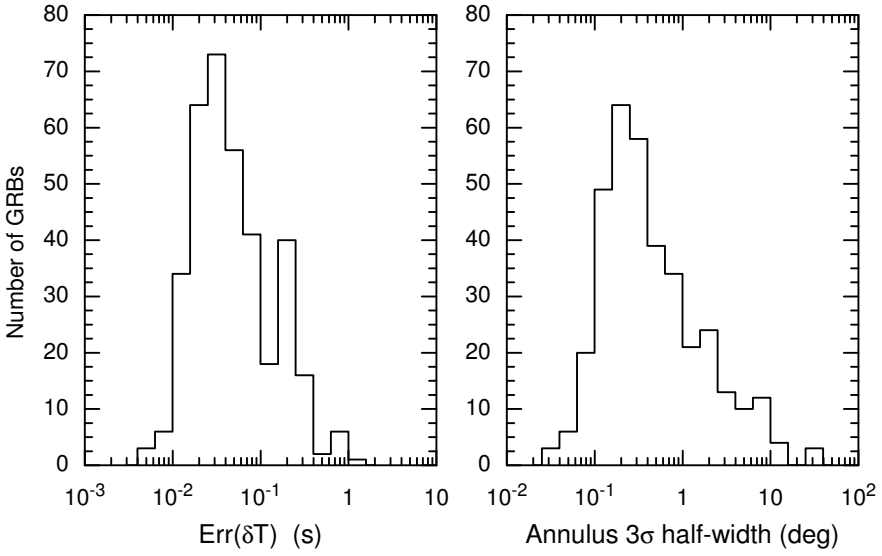

Fig. 4.— Distributions of uncertainties in time delay $d(\delta T) \equiv (d_+(\delta T) + |d_-(\delta T)|)/2$ and 3σ half-widths (HWs) of the 360 triangulation annuli obtained using the Konus-*Wind* and near-Earth (or INTEGRAL) s/c data. The smallest HW is $0\overset{\circ}{.}027$ ($1.6'$), the largest is $32\overset{\circ}{.}2$, the mean is $1\overset{\circ}{.}36$, and the geometrical mean is $0\overset{\circ}{.}45$.

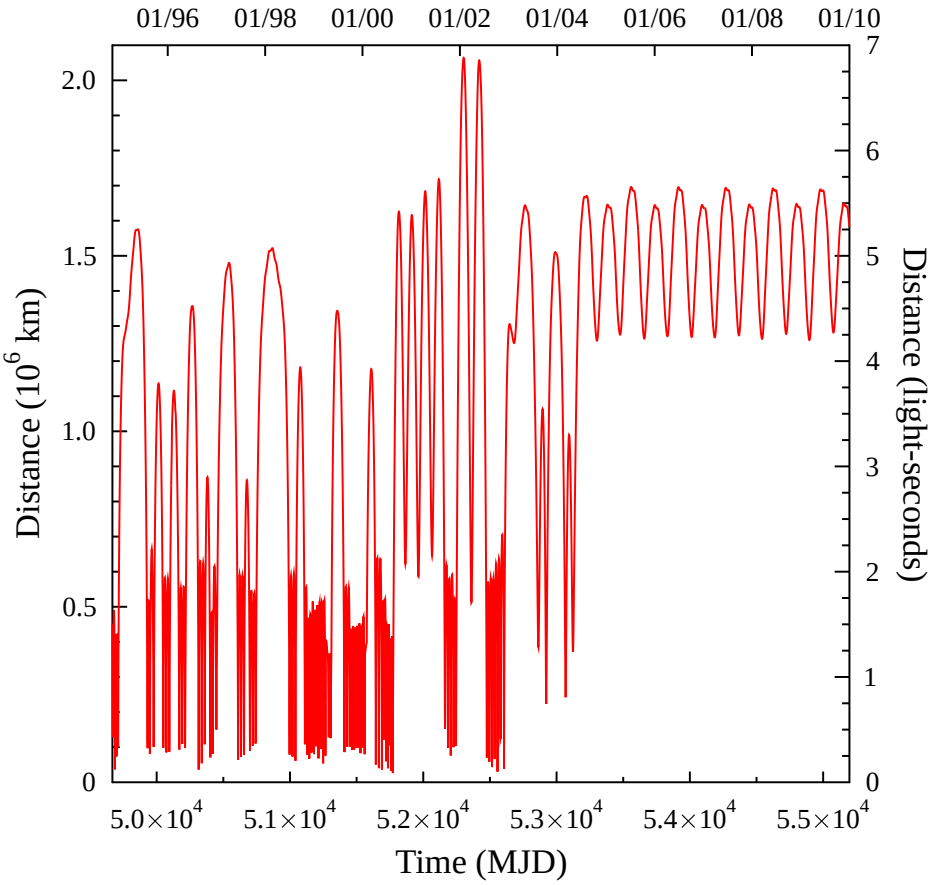

Fig. 5.— *Wind* distance from Earth as a function of time. The maximum distance was ≃7 lt-s in January and May 2002, when it was in a Distant Prograde Orbit (DPO). Since 2004 *Wind* has been in a Lissajous orbit at the L_1 libration point of the Sun-Earth system at a distance of ≃5 lt-s.

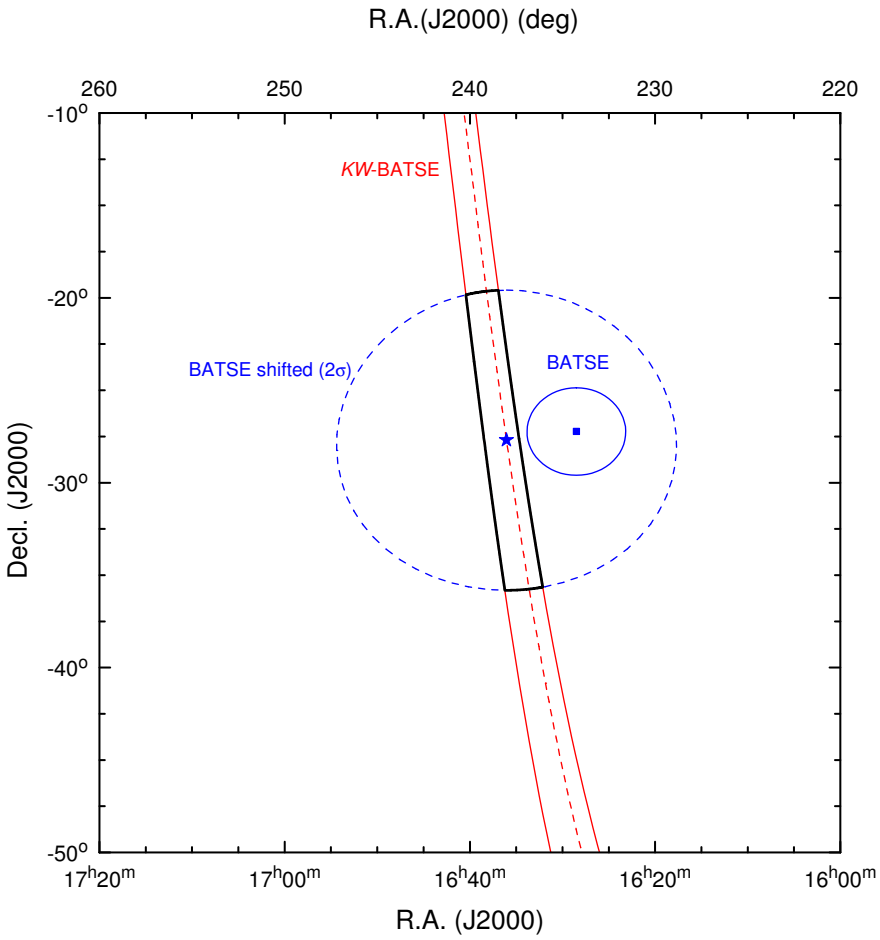

Fig. 6.— IPN/BATSE localization of GRB19960420_T16844 (BATSE #5439). The center of the BATSE error circle (R.A., Decl.(J2000), Err = 234.°25, -27.°23, 2.°37) lies 3.°38 from the center line of the 1.°67 wide KW-BATSE annulus. The resulting long box is shown by the solid black line and its center (that is, the nearest point to the BATSE center at the annulus center line) is indicated by the asterisk. The corners of the box are formed by the intersection of the circle centered at the asterisk with a radius of 8.°12, that is the sum of the 2σ BATSE error radius and 3.°38 systematics (dashed line), and the KW-BATSE annulus.

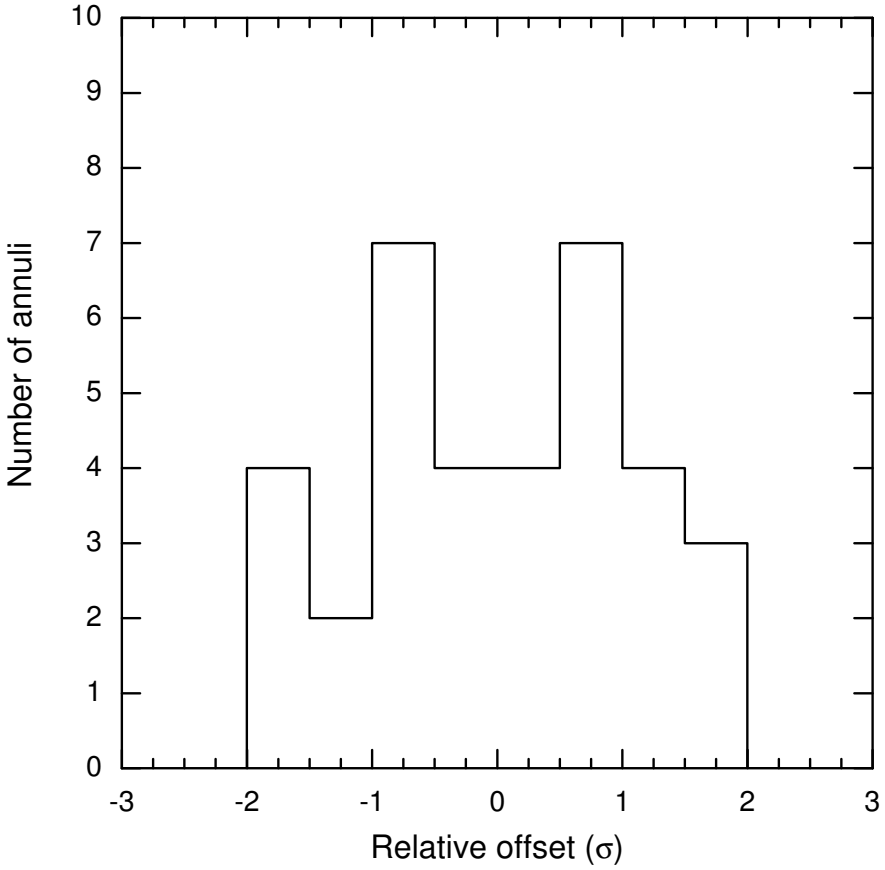

Fig. 7.— Distribution of the offsets of the accurate GRB positions from the center lines of the 35 *KW*-near Earth (or INTEGRAL) s/c annuli.

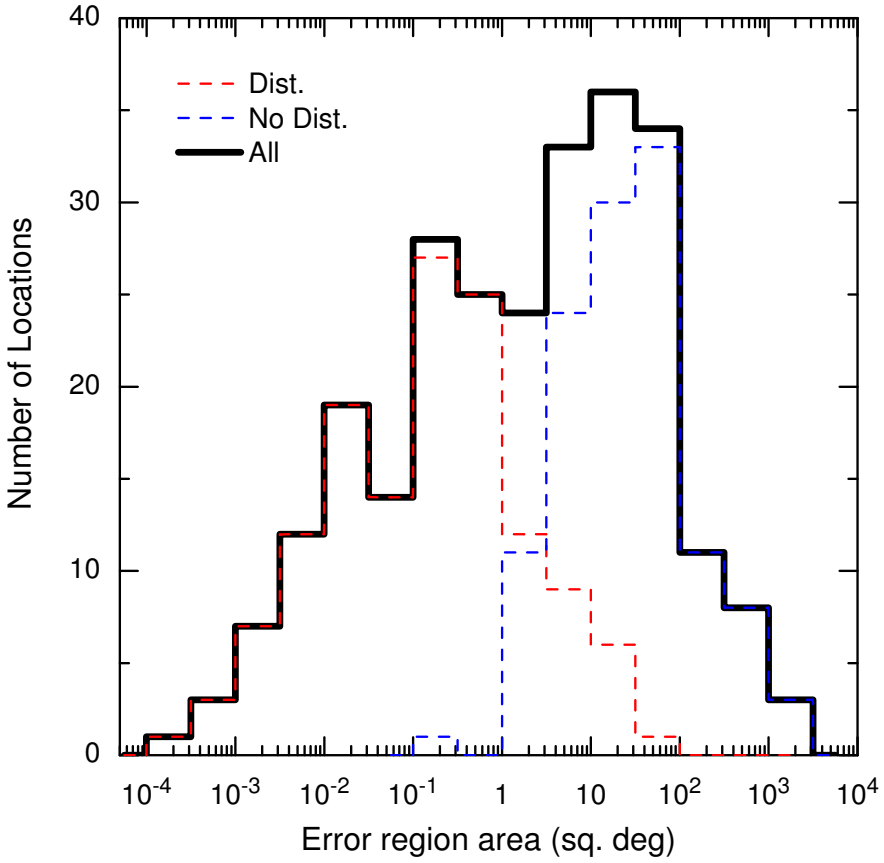

Fig. 8.— Distributions of error region areas for 137 Konus short bursts observed by at least one distant s/c (red dashed line), 121 bursts not observed by any distant s/c (blue dashed line), and all 258 bursts.

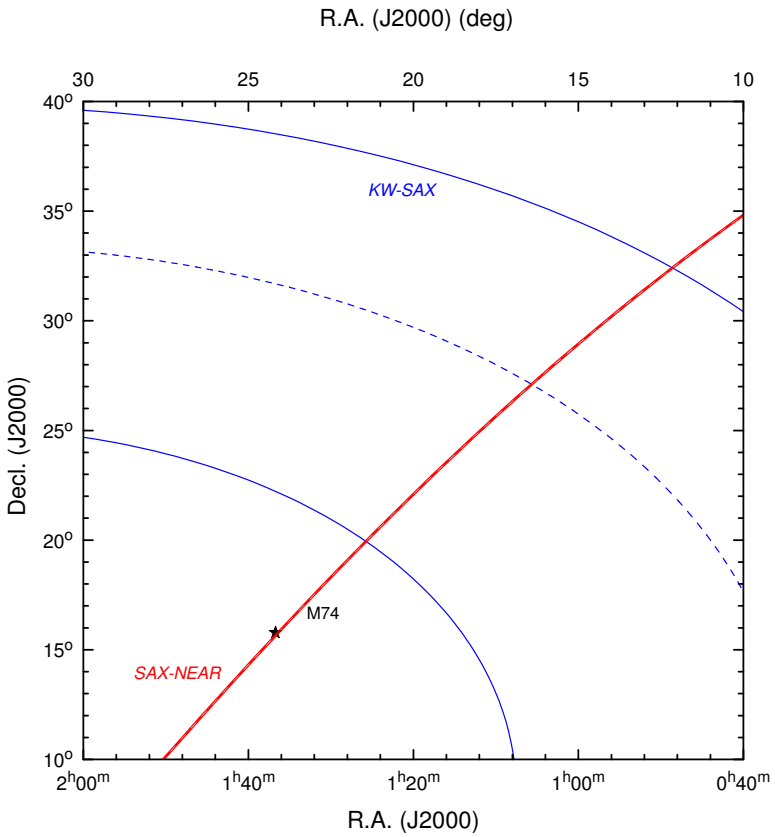

Fig. 9.— IPN localization of GRB 000420 (=GRB20000420_T42714). The 1.7′ wide *SAX-NEAR* annulus passes through the nearby M74 galaxy, while the galaxy is well outside the wide 3σ *KW-SAX* annulus.